Contribution of dislocation dipole structures to the acoustic nonlinearity

W. D. Cash and W. Cai

Citation: J. Appl. Phys. **111**, 074906 (2012); doi: 10.1063/1.3699362
View online: http://dx.doi.org/10.1063/1.3699362
View Table of Contents: http://jap.aip.org/resource/1/JAPIAU/v111/i7
Published by the American Institute of Physics.

Contribution of dislocation dipole structures to the acoustic nonlinearity

W. D. Cash and W. Cai
Department of Mechanical Engineering, Stanford University, Stanford, CA 94305-4040, USA

(Received 7 October 2011; accepted 1 March 2012; published online 10 April 2012)

The ultrasonic nonlinearity created by dislocations in crystals is investigated using two-dimensional dislocation dynamics (DD) simulations. An analytic model of the acoustic nonlinearity parameter, β, of an isolated dislocation dipole is derived using a quasi-static loading assumption. β is predicted to be strongly dependent on the glide stress acting on the dipole, which is not captured by existing models. The technique is extended to an infinite dipole train and an infinite Taylor lattice. β is shown to arise only under the presence of a glide stress. These results contradict the existing model that predicts β of these dipole arrangements to be independent of stress. The analytical models are shown to agree with two-dimensional DD simulations for glide stresses well below the critical stress that causes dissolution of the dipole structure. Several finite sections of the Taylor lattice are modeled with DD and are found to have anomalous scaling behaviors. © *2012 American Institute of Physics*. [http://dx.doi.org/10.1063/1.3699362]

I. INTRODUCTION

One of the ultimate goals of nondestructive evaluation of materials is being able to detect the onset and extent of damage caused by plastic deformation or fatigue. Nonlinear ultrasonics is a technique that is being studied as a promising candidate. Nonlinear ultrasonics was originally used to investigate samples that had undergone a uniaxial deformation,[1] but it has more recently gained attention as a potential way to monitor fatigue damage *in situ*.[2,3]

A major shortcoming of traditional fatigue damage detection techniques is that they are only able to detect macroscopic cracks. In the high-cycle fatigue regime, the vast majority of a metal's life is prior to the emergence of macrocracks.[4] However, the acoustic nonlinearity parameter β has been found to grow in magnitude (by two to four fold) with the number of load cycles in single and polycrystalline metals starting from the early stages of fatigue.[5,6] Thus, nonlinear ultrasonics can potentially monitor the entire fatigue life. Unfortunately, the detailed mechanisms giving rise to the increase of β are not well understood. The anharmonicity of the crystal lattice creates nonlinearities, but its contribution to β remains constant over the range of deformation of interest. The primary contribution to the increase of β is commonly associated the interaction of the ultrasonic waves with dislocations. Throughout the fatigue life, the dislocation density increases substantially and the dislocations spontaneously arrange themselves in various patterns such as veins and persistent slip-bands.[4] Existing analytical models for dislocation contributions to β include a dislocation segment bowing between pinning points in its glide plane and the oscillation of two straight dislocations in a dipole.[5,7,8] The relative weights of these two dislocation effects have not been conclusively determined, but they have already served as the foundation of more advanced models.[9–11]

To date, little had been done to validate these models beyond tenuous links to experiments on bulk specimens. We have recently performed dislocation dynamics (DD) simulations that revealed the shortcomings of the existing model of a bowing dislocation and proposed an improved analytical model that accounts for an orientation-dependent dislocation line energy.[7] DD simulations can reproduce the exact scenario predicted by the improved analytical models. In addition, DD simulations are capable of modeling complex dislocation structures that are beyond the reach of analytical models.

In this paper, a new analytical model of the acoustic nonlinearity for edge-dislocation dipoles is presented. Understanding how dipoles affect β is important, because dipoles are the building block of numerous fatigue microstructures and edge dislocations are the most prevalent in fatigued face-centered cubic (FCC) crystals. The method is extended to include the interactions between dipoles in one- and two-dimensional periodic structures shown in Figs. 1(a) and 1(b). The proposed models are compared with the existing models and 2D DD simulations. DD simulations are then used to predict β for finite sections of the Taylor lattice.

II. ISOLATED DISLOCATION DIPOLE

A. Analytic derivation

The model of the acoustic nonlinearity for an isolated edge dislocation dipole is developed using two infinitely-long edge dislocations gliding in the x-direction as shown in Fig. 2. The glide force per unit length on dislocation 2 at (x, h) due to dislocation 1 with opposite Burgers vector and fixed at the origin is[12]

$$F = \frac{-\mu b^2}{2\pi(1-\nu)} \frac{x(x^2-h^2)}{(x^2+h^2)^2}, \tag{1}$$

where b is the magnitude of the Burgers vector, μ is the shear modulus, and ν is the Poisson's ratio. b is defined as positive when the direction of the Burgers vector for dislocation 1 is in the positive x-direction. Taking a Taylor series expansion

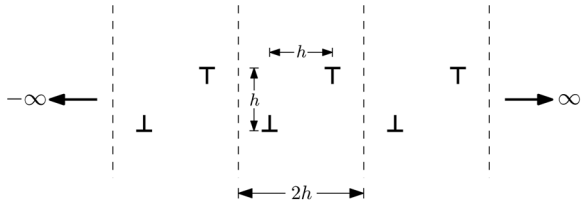

(a) One-dimensional train

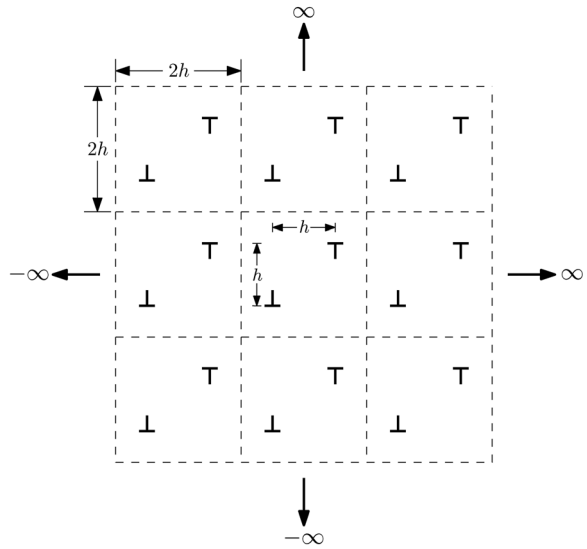

(b) Two-dimensional Taylor lattice

FIG. 1. Relaxed state of infinite dipole structures.

of Eq. (1) about $x = h$, the stable-equilibrium point under zero applied stress, and substituting $\xi = x - h$ to measure displacement of dislocation 2 from the equilibrium point yields

$$F = \frac{-\mu b^2 \xi}{4\pi h^2(1-\nu)} + \frac{\mu b^2 \xi^2}{8\pi h^3(1-\nu)} + \frac{\mu b^2 \xi^3}{8\pi h^4(1-\nu)} + O(\xi^4). \tag{2}$$

The dipole-interaction force required to balance an applied stress σ is

$$F = -\sigma b R, \tag{3}$$

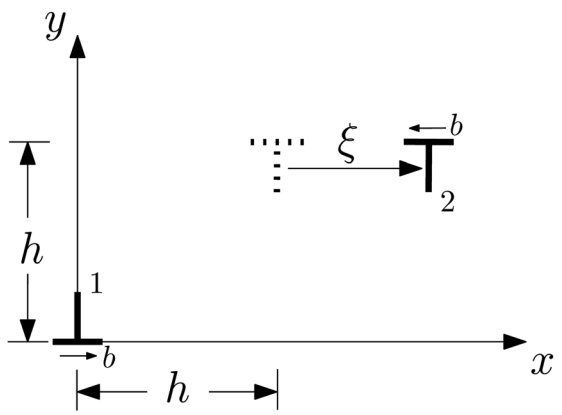

FIG. 2. An isolated dipole gliding in the x-direction. Dislocation 2 is displaced by an amount ξ away from its equilibrium position (h, h), assuming that dislocation 1 is fixed at the origin.

where R is an orientation factor between the applied stress and the resolved shear stress on the glide plane of the dislocations. The strain created by the dipole can be expressed in terms of the dislocation displacement ξ as

$$\epsilon^{dis} = -(\xi b \Lambda)\Omega, \tag{4}$$

where Λ is the dislocation dipole density, and Ω is an orientation factor between the applied and the measured strain component. Here we have assumed that the crystal contains a very low density of dislocation dipoles, so that the interaction between dipoles becomes negligible. Eqs. (2)–(4) provide a relationship between ϵ^{dis} and the applied stress σ.

Given these expressions, β can be obtained using a similar approach as that employed in our previous work,[7] that is from the second derivative of ϵ^{dis} with respect to σ. The dislocation contribution to the acoustic nonlinearity is found to be

$$\beta^{dis} = \frac{-16\pi^2 h^3 \Omega \Lambda R^2 (1-\nu)^2}{b} + \frac{384\pi^3 h^4 \Omega \Lambda R^3 (1-\nu)^3}{\mu b^2}\sigma + O(\sigma^2), \tag{5}$$

the details of the derivation are deferred to the Appendix. To aid in analysis, Eq. (5) can be expressed in non-dimensional form as

$$\frac{\beta^{dis}}{\Lambda b^2} = -16\pi^2 \Omega R^2 (1-\nu)^2 \left(\frac{h}{b}\right)^3 + 384\pi^3 \Omega R^3 (1-\nu)^3 \left(\frac{h}{b}\right)^4 \left(\frac{\sigma}{\mu}\right) + O\left[\left(\frac{\sigma}{\mu}\right)^2\right], \tag{6}$$

where (Λb^2), h/b, and σ/μ are non-dimensional measures of density, glide plane separation, and stress, respectively. Equation (6) can be used to provide an order of magnitude estimate of the dislocation dipole's contribution to acoustic nonlinearity[5] if the dipole density Λ and dislocation spacing h can be estimated from existing transmission electron microscopy studies.[4]

β^{dis} consists of a term independent of applied stress and one that has a linear dependence. The term independent of applied stress in Eq. (6) is identical to the results of Cantrell and Yost,[5] but the linear dependence on stress was missing in the previous expression.[5] This was because in the earlier analysis the Taylor expansions in terms of stress and strain were not carried to sufficiently high order. The mathematics in the approach taken by Cantrell and Yost[5] was very complex, because it started by considering the dynamic wave propagation and only took the quasi-static approximation near the end. In our approach, we take the quasi-static approximation from the very beginning, which greatly simplifies the math and allows us to carry the analysis to much higher order.

B. Numerical simulations

Two-dimensional dislocation dynamics simulations were performed to verify the significance of the newly introduced linear stress dependence and the correctness of the analytical

prediction. A series of simulations were performed for the dislocation structure given in Fig. 2 using DDLab2D, a two-dimensional MATLAB DD code developed by the authors. The stress field of the dislocation was assumed to be that of an infinitely-long, perfect edge dislocation. To reduce the complexity of the simulations, the applied stress was chosen to act directly on the slip system of the dipole and the strain was measured along the slip direction. Therefore, Ω and R are both unity and Eq. (6) reduces to

$$\frac{\beta^{dis}}{(\Lambda b^2)} = -16\pi^2(1-\nu)^2\left(\frac{h}{b}\right)^3 + 384\pi^3(1-\nu)^3\left(\frac{h}{b}\right)^4\left(\frac{\sigma}{\mu}\right). \tag{7}$$

This is the result that will be compared with the DD simulations. Equation (A6) shows that β^{dis} can be calculated in the simulations by taking derivatives of the dislocation strain with respect to stress about the equilibrium stress σ:

$$\beta^{dis} = \frac{\partial^2\epsilon^{dis}}{\partial\sigma^2}\left(\frac{\partial\epsilon}{\partial\sigma}\right)^{-2} = \frac{\partial^2\epsilon^{dis}}{\partial\sigma^2}\left(\frac{1}{\mu}+\frac{\partial\epsilon^{dis}}{\partial\sigma}\right)^{-2} \approx \mu^2\frac{\partial^2\epsilon^{dis}}{\partial\sigma^2}, \tag{8}$$

where again, the dislocation contribution $\partial\epsilon^{dis}/\partial\sigma$ to $\partial\epsilon/\partial\sigma$ is negligible. This assumption has been numerically verified, but the analysis is omitted here. A series of constant-stress simulations were performed to determine the equilibrium dislocation strain ϵ^{dis}. $\partial^2\epsilon^{dis}/\partial\sigma^2$ was then found using a central difference scheme.

The analytical model was compared with the DD simulations of a dipole with $h/b = 10$ in an isotropic material with a Poisson's ratio ν of 0.40. Interactions with other dipoles were ignored. For this configuration, it can be shown from Eq. (1) and Eq. (3) that the critical stress to break the dipole is $\sigma/\mu \approx 6.63 \times 10^{-3}$.

The numerical calculations for β^{dis} are compared with the proposed analytical model and that of Yost and Cantrell[5] in Fig. 3. The DD data show a strong dependence on the applied stress σ. For $\sigma > 2 \times 10^{-3}\ \mu$, β^{dis} changes sign, which has not been captured by previous models. This supports the importance of the term with a linear dependence on σ in the proposed model. The new model agrees well with the DD data for small applied stresses. At higher stresses, β^{dis} deviates from linearity and tends to infinity as σ approaches the critical stress to dissolve the dipole. From Eq. (1), it can be seen that small changes in displacement near the critical distances of $x = (1 \pm \sqrt{2})h$ result in large changes of the interaction forces between the dislocations. Fortunately, the majority of the dipoles in a relaxed microstructure are likely to be acted on by residual stresses well below the dissolution stress. It should also be noted that the β^{dis} is asymmetric about the vertical axis ($\sigma = 0$), as one would expect from the asymmetric structure of an edge-dislocation dipole.

III. INFINITE DIPOLE TRAIN

A. Analytic derivation

To better approximate realistic dislocation structures it is necessary to consider the interaction of dislocations in multipolar structures. The simplest stable case to consider is that of the infinite dipole train shown in Fig. 1(a). Although stable in the infinite limit (i.e., under periodic boundary condition (PBC)), a finite dipole train's stability depends on its end conditions. It is easy to verify by symmetry that the relaxed spacing between neighboring dislocations is exactly that of an isolated dipole; each dislocation is separated from it is nearest neighbors by a distance h in the glide plane and h normal to the glide plane. It is also evident that dislocations with the same Burgers vector will have identical displacements, $\xi/2$, due to an applied stress below the critical stress to dissolve the structure. Likewise, dislocations of the opposite Burgers vector will displace by $-\xi/2$.

These homogeneous displacements allow β to be calculated by considering the nonlinearities that arise from a single dislocation of Burgers vector b interacting with every dislocation of opposite sign, as shown in Fig. 4. The β calculated for this structure is that of the entire dipole train if the dislocation dipole density Λ is taken to be

$$\Lambda = \frac{1}{hd}, \tag{9}$$

where d is the distance normal to the glide plane between neighboring trains. Here we assume that d is large enough for the interactions between dipole trains to be negligible.

Unfortunately, β cannot be directly calculated by summing the contribution from each dislocation pair in the dipole train, because it is evident in Eq. (A6) that β^{total} does not satisfy linear superposition. However, the stress and strain fields of these dislocations can be summed to calculate the acoustic nonlinearity of the entire structure. As with the isolated dislocation model, a stress σ is applied and resulting strain is calculated for the entire structure. The forces to counteract the applied load are found by considering the stress fields created by individual dislocations. Performing this sum numerically requires an infinite summation that must be truncated.

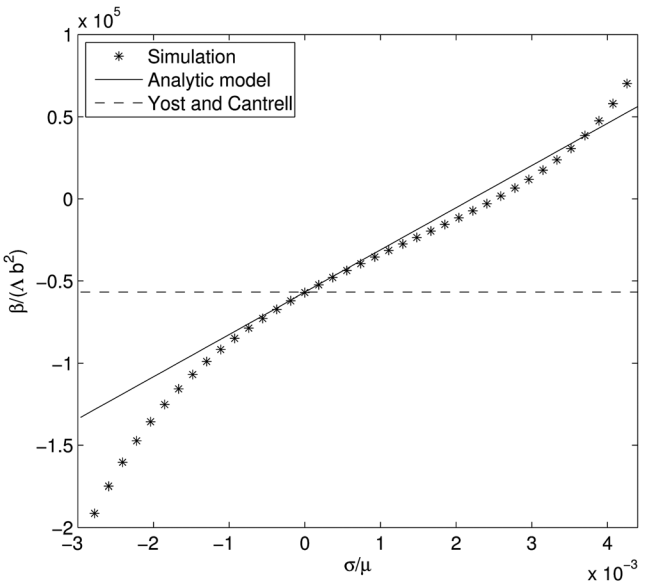

FIG. 3. Non-dimensional β of an isolated dipole from DD simulations (*) compared with the analytic results derived here (solid line) and the results of Cantrell and Yost[5] (dashed line).

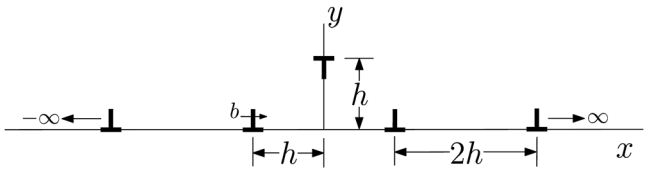

FIG. 4. Single dislocation acted on by a wall of oppositely signed dislocations.

Fortunately, the analytical solution of the stress fields created by tilt grain boundaries can be used instead.[12]

The stress field of the infinite wall in Fig. 4 with dislocations separated by $2h$ along the x-axis is

$$\sigma_{xy} = \sigma_o \sin 2\pi X(\cosh 2\pi Y + \cos 2\pi X - 2\pi Y \sinh 2\pi Y), \tag{10}$$

where

$$\sigma_o = \frac{\mu b}{4h(1-\nu)(\cosh 2\pi Y + \cos 2\pi X)^2}, \tag{11}$$

with $X = x/2h$ and $Y = y/2h$. Because the height of the dipole train is always $y = h$, Y can be simplified to 1/2.

Using the technique for the isolated dipole in the Appendix, a Taylor series expansion of the stress is

$$\sigma_{xy} = \frac{c_1 \mu \epsilon^{dis}}{h^2 \Omega \Lambda R(1-\nu)} + \frac{c_2 \mu \epsilon^{dis^3}}{b^2 h^4 \Omega^3 \Lambda^3 R(1-\nu)} + O(\xi^5), \tag{12}$$

where the constants c_1 and c_2 are

$$c_1 = \frac{\pi[\pi \sinh(\pi) - \cosh(\pi) - 1]}{4[\cosh(\pi) + 1]^2} = 0.117344, \tag{13}$$

$$c_2 = \frac{\pi^3[\cosh(\pi)^2 - \cosh(\pi) - \pi\cosh(\pi)\sinh(\pi) + 5\pi\sinh(\pi) - 2]}{24[\cosh(\pi) + 1]^3} = -0.0766042. \tag{14}$$

The acoustic nonlinearity from both the lattice and dislocations, β^{total}, can then be found to be

$$\begin{aligned}\beta^{\text{total}} &= \frac{\partial^2 \epsilon}{\partial \sigma^2}\left(\frac{\partial \epsilon}{\partial \sigma}\right)^{-2} \\ &= \frac{\frac{-A_{666}}{A_{66}^3} + \frac{c_2}{c_1^4}\frac{h^4 \Omega \Lambda R^3 (1-\nu)^3}{\mu^3 b^2}\sigma}{\left(\frac{1}{A_{66}} + \frac{h^2 \Omega \Lambda R(1-\nu)}{c_1 \mu}\right)^2} + O(\sigma^3).\end{aligned} \tag{15}$$

If the dislocation density is assumed to be sufficiently small, it can again be verified that

$$\frac{h^2 \Omega \Lambda R(1-\nu)}{c_1 \mu} \ll \frac{1}{A_{66}}. \tag{16}$$

By removing the lattice contribution and simplifying, the dislocation contribution in nondimensional form is

$$\begin{aligned}\frac{\beta^{dis}}{(\Lambda b^2)} &= \frac{c_2}{c_1^4}\Omega R^3 (1-\nu)^3 \left(\frac{h}{b}\right)^4 \left(\frac{\sigma}{\mu}\right) \\ &= 2424.19 \Omega R^3 (1-\nu)^3 \left(\frac{h}{b}\right)^4 \left(\frac{\sigma}{\mu}\right).\end{aligned} \tag{17}$$

Equation (17) reveals that β^{dis} has a linear stress dependence for both the isolated dipole and the the train, but the train lacks a stress independent term. The absence of this term is a result of the symmetry of the train. The proposed β^{dis} contradicts the model of Cantrell and Yost[5], which claims that β^{dis} of dipole patterns is a multiple of stress-independent contributions from isolated dipoles.

B. Numerical results

Numerical simulations of the dipole train were performed using the technique and material properties described in Sec. II B. A dipole was modeled in a domain of width $2h$ in the glide plane. An infinite train was simulated by using a PBC along the direction of the train, similar to the schematic in Fig. 1(a). The simulation results are plotted over a range of applied stresses in Fig. 5. The numerical results agree closely with the proposed analytical model. β^{dis} is found to be zero under no applied stress in the DD simulations, which supports the models prediction that there is no stress independent term for the train. A lack of a stress independent β^{dis}

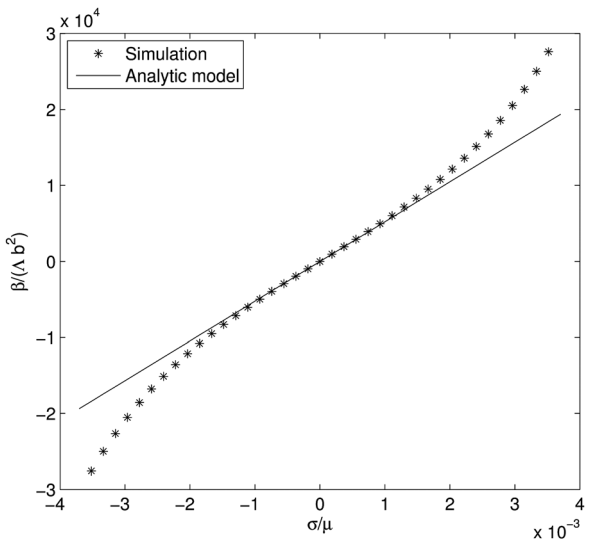

FIG. 5. Non-dimensional β of an infinite dipole train (*) from DD simulations compared with our analytic prediction (solid line).

is an important difference between the train and the isolated dipole. Another difference is that the data for the train are antisymmetric about zero applied stress, that is

$$\beta^{dis}(-\sigma) = -\beta^{dis}(\sigma). \tag{18}$$

Figure 3 shows that this is not the case for the isolated dipole, even if the offset at zero stress is removed. This further illustrates the importance of the symmetry of the dislocation structure.

IV. INFINITE TWO-DIMENSIONAL LATTICE

A. Analytic derivation

The interaction of dipoles can be further extended to two dimensions by considering the infinite lattice in Fig. 1(b). This 2D structure is stable in the infinite limit (i.e., under PBC), but the stability of finite 2D structures (see Sec. V) depends on the shape of the structure.[13] It is again easy to verify from symmetry that the relaxed spacing between neighboring dislocations is h in both the glide plane and the normal direction. Similar to the train, the displacement of dislocations is identical for all dislocations with the same Burgers vector. Thus, β^{dis} can again be calculated by considering the interaction of a single dislocation with all others of opposite sign, as shown in Fig. 6. Again, the β of individual pairs of dislocations cannot be summed; the stress and strain fields of the entire structure must be calculated, instead. Unfortunately, there is not an existing analytical stress field for this structure. The solution can be obtained by an analytic sum over one dimension and numerical summation over the other dimension.

The stress field of a dislocation wall given in Eq. (10) will again be used, but now Y will vary based on the distance normal to the glide plane between the dislocation at the origin and the given wall. From Fig. 6 can see that

$$Y = \pm\frac{h(2i-1)}{2h} = \pm(i-1/2) \qquad i = 1,2,3\ldots, \tag{19}$$

where i is the pair number, as shown in Fig. 6, and the sign depends on if the dislocation at the origin is above or below the given wall. Similar to the dipole train, the stress field for each dislocation wall can be expressed as a Taylor series

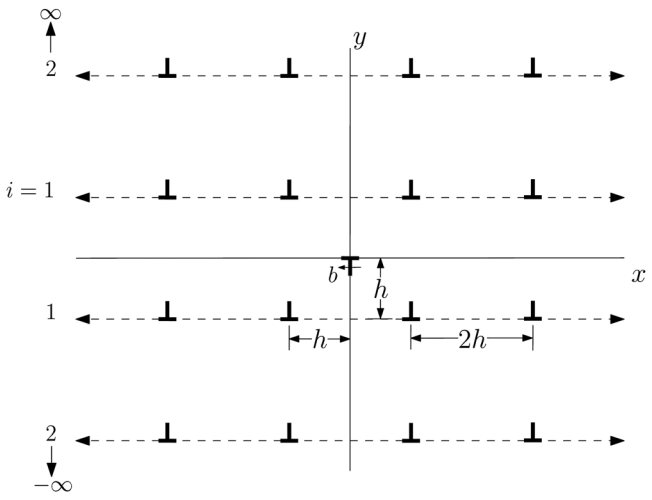

FIG. 6. Single dislocation acted on by an infinite lattice of oppositely-signed dislocation walls.

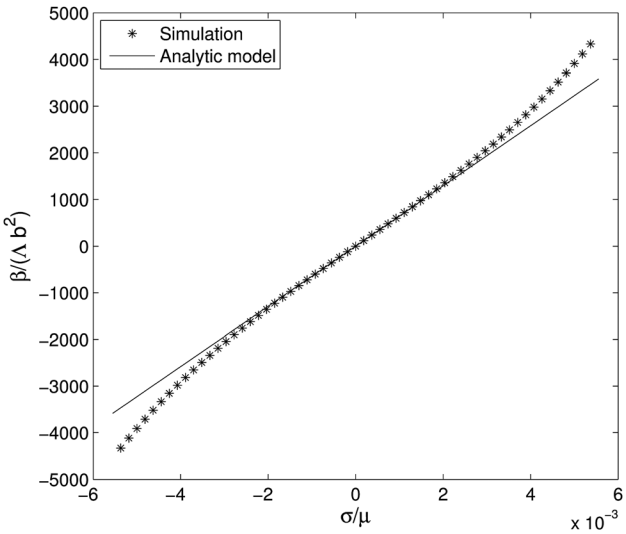

FIG. 7. Non-dimensional β of an infinite 2D lattice from DD simulations (*) compared with our analytic predictions (solid line).

expansion about $x = 0$. The stress fields can then be summed and solved using the same technique. While the dislocation density within a Taylor lattice considered here is very high, we assume that such a lattice still occupies only a small region of a real crystal, as would be the case for fatigue veins. Hence, the overall density Λ is much smaller than $1/(2h^2)$, and Eq. (16) is satisfied. In this case, β^{dis} can again be expressed by Eq. (17), but with $c_1 = 0.236829$, $c_2 = -0.940371$, so that $c_2/c_1^4 = 298.922$. The constants depend on where the infinite summation of dislocation walls is truncated; fortunately, c_1 and c_2 converge with only a few pairs of dislocations walls.

As with the dipole train, the symmetry of the 2D dislocation lattice causes there to be no stress independent contribution to the acoustic nonlinearity. This is again in disagreement with the Cantrell and Yost model[5] that predicts β^{dis} to be independent of applied stress and a multiple of their isolated dipole model. Another important observation is that the coefficient c_2/c_1^4 for the 2D lattice is about ten times than smaller that of the 1D train. Thus, how dislocations pattern themselves, for example, the emergence of persistent slip bands from fatigue veins, can drastically affect the acoustic nonlinearity.

B. Numerical simulations

Only minor modifications to the dipole train simulations had to be made to model the 2D dislocation lattice. A single dipole was again modeled, but a square domain of size $2h$ with periodic boundary conditions in both directions was used, as illustrated in Fig. 1(b). DDLab2D computes the stress field of a dislocation in 2D periodic domain using the same technique employed in the analytical model—a finite summation of pairs of dipole walls. The summation was truncated after 20 pairs. For the assumption in Eq. (16) to be valid, the dislocation density in the crystal was assumed to be much smaller than the actual density in the simulation domain.

The simulation results are plotted over a range of applied stresses in Fig. 7. There is a strong agreement with the proposed analytical model and β^{dis} lacks a stress independent term. Similar to the dipole train, the numerical data are antisymmetric about zero applied stress for the 2D lattice.

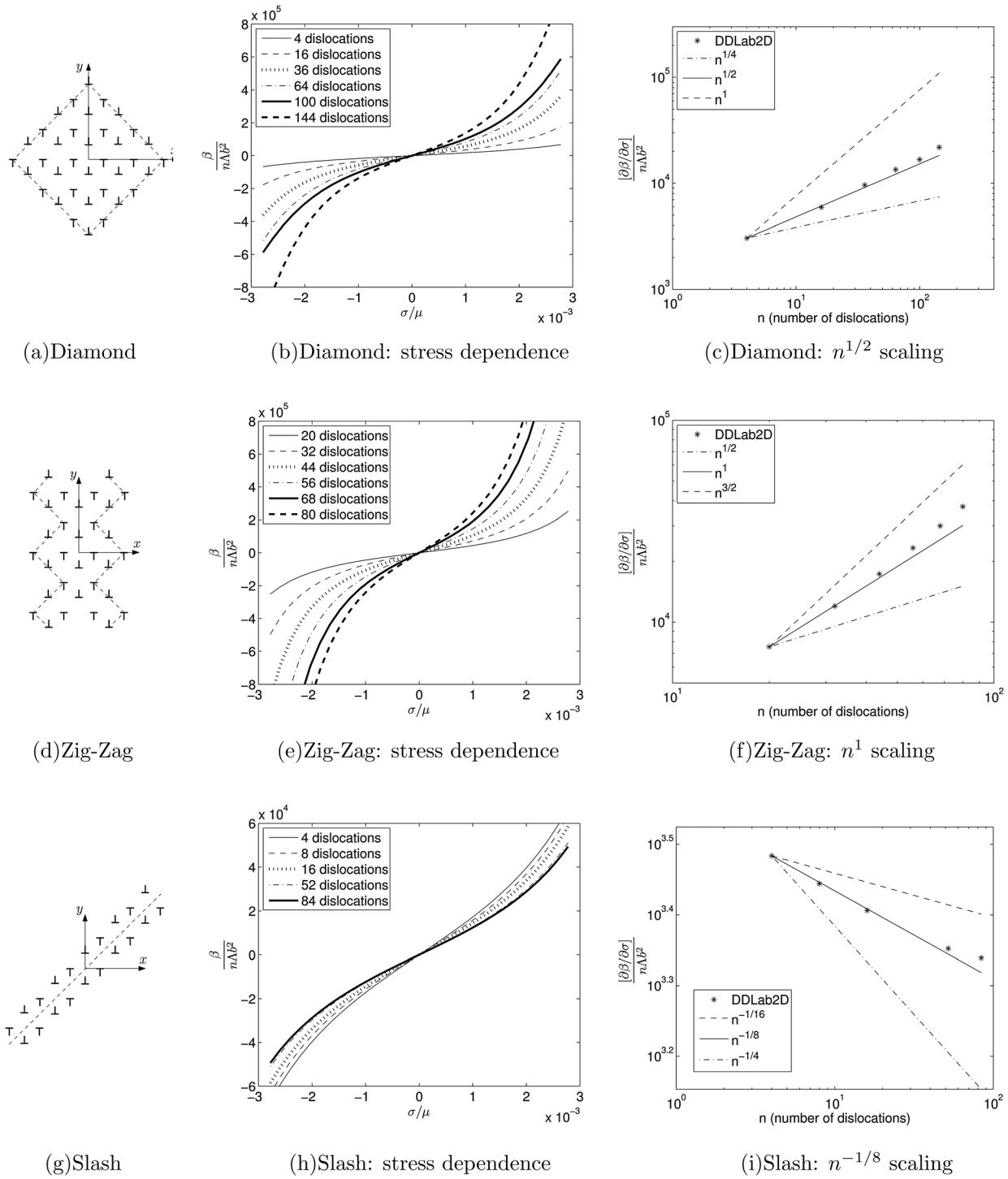

(a)Diamond (b)Diamond: stress dependence (c)Diamond: $n^{1/2}$ scaling

(d)Zig-Zag (e)Zig-Zag: stress dependence (f)Zig-Zag: n^{1} scaling

(g)Slash (h)Slash: stress dependence (i)Slash: $n^{-1/8}$ scaling

FIG. 8. The stress dependence of acoustic non-linearity for three stable, finite dipole structures studied in this work. The left column shows the schematics of three structures: (a) diamond, (d) zig-zag, (g) slash. The middle column shows the non-dimensionalized acoustic non-linearity as a function of stress for the three structures of different sizes. The right column shows the size scaling of the stress dependence of β (i.e., $\partial\beta/\partial\sigma$) near zero stress for the three structures.

V. FINITE TWO-DIMENSIONAL LATTICES

The previous sections have highlighted how the acoustic nonlinearity is affected by the interactions between dipoles. Considering finite dipolar structures in Fig. 8 is a natural extension of this study. The diamond structure in Fig. 8(a) is a commonly used approximation of a fatigue vein.[4] The zig-zag structure in Fig. 8(d) is elongated along the y-axis and might be used to approximate the structure within a persistent slip band. All three arrangements considered are extracted from the infinite Taylor lattice. Each one is composed solely of elementary quadrupoles, and thus satisfies Neumann's stability condition.[14]

The contribution to β from dislocations on the boundary of the lattices may be significantly different than those in the interior and could lead to a size dependence. Unfortunately, deriving analytical models using the presented techniques is unfeasible, because it would require considering the

interactions of every pair of dislocations in every configuration. However, β can still be easily calculated using DD simulations.

The dependence of β on applied stress over a variety of structure sizes are plotted in the second column of Fig. 8 for all three shapes. To account for the varying structure size, the non-dimensional acoustic nonlinearity is redefined as

$$\frac{\beta^{dis}}{n(\Lambda b^2)}, \tag{20}$$

where n is the number of dislocations in each structure and the density λ is held constant. The curves are qualitatively similar to those in the previous sections. Once again, all of these structures have no acoustic nonlinearity at zero applied stress. All three shapes exhibit a size dependence, but to varying degrees. The slope of the curves about zero applied stress,

$$\left.\frac{d\beta/n(\Lambda b^2)}{d\sigma/\mu}\right|_{\sigma=0} \tag{21}$$

is plotted against n in the third column of Fig. 8 to better quantify the effect. Each shape is shown to have a well-defined scaling with a power of n. If there were no size effect, the normalized slope would be independent of n, i.e., n^0 scaling. The normalized slope of the diamond and zig-zag structure are shown to be proportional to $n^{1/2}$ and n^1, respectively, while that of the slash actually decreases at a rate of $n^{-1/8}$. It should also be noted that the four dislocation structure for the diamond and slash are the same and have identical acoustic nonlinearity, as shown in Figs. 8(b) and 8(h).

The reasons for the exact scaling exponent in each case are not clear. However, the general behavior is likely a result of how much the structure deforms as its breakdown stress is reached. Both the diamond and zig-zag structures undergo a large amount of deformation prior to failure. The relative displacement of the dislocations increases as the number of dislocations in the cluster increases. In the largest clusters, the quadrupole structures tend to decompose into dipole walls under as the stress approaches the breakdown stress. Both of these effects likely cause $(\partial\beta/\partial\sigma)/(n\Lambda b^2)$ to increase with increasing n. On the other hand, the quadrupoles in the slash structure remain intact under stress. The quadrupoles in the larger slashes appear to deform even less under stress, which may explain the decrease of $(\partial\beta/\partial\sigma)/(n\Lambda b^2)$ with increasing n.

VI. CONCLUSIONS

The analytical models presented in this paper offer an improvement over the existing model on acoustic nonlinearity β arising from dislocation dipoles and multipoles. Both the analytic models and DD simulations show a strong stress dependence of β. The inclusion of the stress dependence term also allows for the possibility of a decrease, or even a change of sign, of the dislocation contribution to β when an external stress is applied. A similar effect was recently discovered for a dislocation bowing between pinning points.[7] An important difference is that for the bowing dislocation this effect depends on the material's Poisson's ratio, whereas the effect considered here is relatively insensitive to the Poisson's ratio. Furthermore, among the many structures considered here, only isolated dipoles have a non-zero β at zero stress. All other structures give zero β at zero stress. This difference between isolated dislocation dipoles and multipolar structures could be particularly important when considering the fatigue microstructures of veins and persistent slip-bands.

Both our previous model for a pinned dislocation[7] and that presented here show a strong dependence on the applied stress σ. Unfortunately, there have been few experiments to measure how β depends on the stress applied to the sample, with the exception of the work of Hikata *et al.*[1] The methods they used on uniaxially strained samples could be easily extended to single and polycrystalline samples at various stages of their fatigue life. We hope more experiments will be conducted in the future to measure the effect of externally applied stress on acoustic non-linearity. The comparison between experimental data and theoretical predictions is likely to lead to a better understanding of the fundamental mechanics of acoustic nonlinearity and possibly a method to extract more information about the types of dislocation patterning in the sample.

A major conclusion of this work is that β depends not only on the number of the dislocations, but also on how they are arranged spatially. DD simulations are particularly well suited for predicting the acoustic nonlinearity from large dislocation structures for which analytic solutions are difficult to find. Our longer term goal is to use 3-dimensional DD simulations to predict acoustic nonlinearity due to more realistic dislocation microstructures typically found in metals after uniaxial or cyclic plastic deformations.

ACKNOWLEDGMENTS

This work is funded by the Air Force Office of Scientific Research Grant FA9550-07-1-0464. W. D. Cash is supported by the Benchmark Stanford Graduate Fellowship. The authors would like to thank D. M. Barnett and W. D. Nix for their invaluable advice.

APPENDIX: DERIVATION OF β FROM AN ISOLATED DISLOCATION DIPOLE

Following the technique presented in Ref. 7 to solve for the acoustic nonlinearity, Eqs. (3) and (4) are substituted into Eq. (2) to give

$$\sigma = \frac{\mu\epsilon^{dis}}{4\pi h^2\Omega\Lambda R(1-\nu)} + \frac{\mu\epsilon^{dis^2}}{8\pi b h^3\Omega^2\Lambda^2 R(1-\nu)} - \frac{\mu\epsilon^{dis^3}}{8\pi b^2 h^4\Omega^3\Lambda^3 R(1-\nu)} + O(\epsilon^{dis^4}). \tag{A1}$$

Taking a series reversion to express ϵ^{dis} as a function of σ yields

$$\epsilon^{dis} = \frac{4\pi h^2\Omega\Lambda R(1-\nu)}{\mu}\sigma - \frac{8\pi^2 h^3\Omega\Lambda R^2(1-\nu)^2}{\mu^2 b}\sigma^2 - \frac{64\pi^3 h^4\Omega\Lambda R^3(1-\nu)^3}{\mu^3 b^2}\sigma^3 + O(\sigma^4). \tag{A2}$$

In addition to the strain due to dislocation motion, the applied stress creates an elastic lattice strain that can be expressed as

$$\epsilon^{lat} = \frac{\partial u_1}{\partial x_2} = \frac{1}{A_{66}}\sigma - \frac{1}{2}\frac{A_{666}}{A_{66}^3}\sigma^2, \tag{A3}$$

where A_{66} and A_{666} are the second- and third-order elastic stiffness in Voigt notation, respectively. The total strain ϵ is thus the summation of the elastic lattice strain and the strain of the dislocation

$$\begin{aligned}\epsilon &= \epsilon^{lat} + \epsilon^{dis} \\ &= \left(\frac{1}{A_{66}} + \frac{4\pi h^2 \Omega \Lambda R(1-\nu)}{\mu}\right)\sigma \\ &\quad - \left(\frac{1}{2}\frac{A_{666}}{A_{66}^3} + \frac{8\pi^2 h^3 \Omega \Lambda R^2 (1-\nu)^2}{\mu^2 b}\right)\sigma^2 \\ &\quad + \frac{64\pi^3 h^4 \Omega \Lambda R^3 (1-\nu)^3}{\mu^3 b^2}\sigma^3 + O(\sigma^4).\end{aligned} \tag{A4}$$

In order to measure the acoustic nonlinearity, a small-amplitude wave is generated by an ultrasonic transducer. The dynamic propagation of the wave can be ignored, because inertial effects on the dislocations will be negligible in the frequency range of interest (0.1–100 MHz) and because the stresses created by the transducer is very small. The system can instead be modeled using a quasi-static loading assumption; the assumption has been used in previous analytical models and greatly reduces the complexity of the simulations.[7,8] The transducer creates a small oscillatory stress of amplitude $\Delta\sigma$ in addition to the static stress σ. At equilibrium, an additional strain $\Delta\epsilon$ is created in response to the change in stress. This can be represented as

$$\begin{aligned}\Delta\sigma &= \frac{\partial\sigma}{\partial\epsilon}\Delta\epsilon + \frac{1}{2}\frac{\partial^2\sigma}{\partial\epsilon^2}(\Delta\epsilon)^2 + \cdots \\ &= \left(\frac{\partial\epsilon}{\partial\sigma}\right)^{-1}\Delta\epsilon - \frac{1}{2}\frac{\partial^2\epsilon}{\partial\sigma^2}\left(\frac{\partial\epsilon}{\partial\sigma}\right)^{-3}(\Delta\epsilon)^2 + \cdots,\end{aligned} \tag{A5}$$

where the derivatives of ϵ can be derived from Eq. (A4). It can be shown from Eq. (A5) that the total acoustic nonlinearity parameter β^{total} is

$$\beta^{\text{total}} = \frac{\partial^2\epsilon}{\partial\sigma^2}\left(\frac{\partial\epsilon}{\partial\sigma}\right)^{-2} = \frac{\dfrac{-A_{666}}{A_{66}^3} - \dfrac{16\pi^2 h^3 \Omega \Lambda R^2 (1-\nu)^2}{\mu^2 b^2} + \dfrac{384\pi^3 h^4 \Omega \Lambda R^3 (1-\nu)^3}{\mu^3 b^2}}{\left(\dfrac{1}{A_{66}} + \dfrac{4\pi h^2 \Omega \Lambda R(1-\nu)}{\mu}\right)^2} + O(\sigma^2). \tag{A6}$$

In most cases

$$\frac{4h^2\pi\Omega\Lambda R(1-\nu)}{\mu} \ll \frac{1}{A_{66}}. \tag{A7}$$

Equation (A6) can thus be simplified to

$$\beta^{\text{total}} = \frac{-A_{666}}{A_{66}^3} + \frac{16\pi^2 h^3 \Omega \Lambda R^2 (1-\nu)^2 A_{66}^2}{\mu^2 b} + \frac{384\pi^3 h^4 \Omega \Lambda R^3 (1-\nu)^3 A_{66}^2}{\mu^3 b^2}\sigma + O(\sigma^2), \tag{A8}$$

where A_{666}/A_{66} is the lattice contribution to β^{total}. A_{666}/A_{66} is invariant over the range of interest and will henceforth be omitted. After removing the lattice contribution and recognizing that A_{66} is simply the shear modulus μ in an isotropic medium, the dislocation component of β is

$$\beta^{dis} = \frac{-16\pi^2 h^3 \Omega \Lambda R^2 (1-\nu)^2}{b} + \frac{384\pi^3 h^4 \Omega \Lambda R^3 (1-\nu)^3}{\mu b^2}\sigma + O(\sigma^2) \tag{A9}$$

which is identical to Eq. (5).

[1] A. Hikata, B. B. Chick, and C. Elbaum, Appl. Phys. Lett. **3**, 195 (1963).
[2] P. B. Nagy, Ultrasonics **36**, 375 (1998).
[3] J.-Y. Kim, L. J. Jacobs, J. Qu, and J. W. Littles, J. Acoust. Soc. Am. **120**, 1266 (2006).
[4] S. Suresh, *Fatigue of Materials* (Cambridge University Press, 1998).
[5] J. H. Cantrell and W. T. Yost, Philos. Mag. A **64**, 315 (1994).
[6] J. Frouin, S. Sathish, and J. K. Na, Proc. SPIE **3993**, 60 (2000).
[7] W. D. Cash and W. Cai, J. Appl. Phys. **109**, 014915 (2011).
[8] A. Hikata, B. B. Chick, and C. Elbaum, J. Appl. Phys. **36**, 1 (1965).
[9] J. H. Cantrell, Proc. R. Soc. Lond. A **460**, 757 (2004).
[10] J. H. Cantrell, J. Appl. Phys. **105**, 043520 (2009).
[11] R. K. Oruganti, R. Sivaramanivas, T. N. Karthik, V. Kommareddy *et al.*, Int. J. Fatigue **29**, 2032 (2007).
[12] J. P. Hirth and J. Lothe, *Theory of Dislocations* (Wiley, New York, 1982).
[13] F. R. N. Nabarro, Mater. Sci. Eng. A **317**, 12 (2001).
[14] P. Neumann, Mat. Sci. Eng. **81**, 465 (1986).